



Cite this: *RSC Adv.*, 2023, **13**, 28042

Unravelling the surface structure of $\beta\text{-Ga}_2\text{O}_3$ (100)

Alex Sandre Kilian,^a Abner de Siervo,^{id}^b Richard Landers,^b Guilherme Jean P. Abreu,^{id}^c Mayron S. Castro,^b Tyson Back,^{id}^d and Alexandre Pancotti^{id}^{*a}

The present work is on a comprehensive surface atomic structure investigation of $\beta\text{-Ga}_2\text{O}_3$ (100). The $\beta\text{-Ga}_2\text{O}_3$ single crystal was studied by a structural model system in the simulations and *in situ* characterization via X-ray photoelectron spectroscopy (XPS), low-energy electron diffraction (LEED) and X-ray photoelectron diffraction (XPD) allowed for probing the outermost layers' properties. *In situ* XPD characterization allows for the collection of valuable element-specific short-range information from the $\beta\text{-Ga}_2\text{O}_3$ surface, and the results were compared to a systematic and precise multiple scattering simulation approach. The experiments, characterizations, and simulations indicated strong evidence of considerable structural variations in the interatomic layer's distances. Such atomic displacement could clarify the electronic phenomena observed in theoretical studies. The comparison between experimental and theoretical XPD results involving multiple scattering calculations indicated that the $\beta\text{-Ga}_2\text{O}_3$ surface has two possible terminations. The best fits to the photoelectron diffraction curves are used to calculate the interplanar relaxation in the first five atomic layers. The results show good agreement with previous density functional theory calculations, establishing XPD as a useful tool for probing the atomic structure of oxide surfaces.

Received 12th July 2023
 Accepted 8th September 2023
 DOI: 10.1039/d3ra04682f
rsc.li/rsc-advances

Introduction

Ga_2O_3 is an ultrawide bandgap (UWBG) semiconductor oxide material, with an ultrawide-bandgap (UWBG) ranging from 4.5–5.3 eV. Compared to other semiconductor materials, for example SiC (3.3 eV) and GaN (3.4 eV), Ga_2O_3 has a larger band gap, and good chemical stability. Additionally, Ga_2O_3 has a theoretical breakdown electric field at 8 MV cm⁻¹, being three times larger than that of either SiC or GaN, and a large Baliga's figure of merit (BFOM).¹ This makes Ga_2O_3 particularly useful for power electronic applications, where extreme environments such as high temperature, high radiation, high voltage, and high current are a concern. For these reasons, Ga_2O_3 has been investigated for use in power transmission, rail traction, hybrid propulsion, rail guns, and Schottky barrier diodes.^{2–4}

Ga_2O_3 is a polymorph material that can have six crystalline phases, known as α , β , γ , δ , ε and κ . The $\beta\text{-Ga}_2\text{O}_3$ is the most stable thermodynamically, even at 2023 K. The formation energy of the polymorphs has the following order $\beta < \varepsilon < \alpha < \delta < \gamma$.³

^aInstituto de Ciências Exatas e Tecnológicas/Grupo de Física de Materiais, Universidade Federal de Jataí, BR 364, km 195, No. 3800, 75801-615, Jataí, Goiás, Brazil. E-mail: apancotti@ufj.edu.br

^bInstituto de Física "Gleb Wataghin", Universidade Estadual de Campinas, Campinas 13083-859, SP, Brazil

^cDepartamento de Física, Universidade Federal do Paraná, Caixa Postal 19044, 81531-980, Curitiba-PR, Brazil

^dAir Force Research Laboratory, 2179 12th Street, B652/R122, WPAFB, Ohio 45433-7718, USA

$\beta\text{-Ga}_2\text{O}_3$ has the monoclinic structure with the space group $C2/m$ or C_{2h}^3 space group (number 12).⁵ Fig. 1 shows the conventional unit cell of $\beta\text{-Ga}_2\text{O}_3$. The Ga atoms are at two crystallographic inequivalent positions, one in the tetrahedral geometry Ga(i), and the other in the octahedral geometry Ga(ii). The oxygen ions are arranged in three crystallographic different positions O(i), O(ii), and O(iii), where O(i) and O(ii) oxygen atoms are coordinated trigonally and O(iii) is coordinated tetrahedrally, all of them situated at $4i(x,0,z)$ positions at the C_s group symmetry plane. The crystalline structure may be described as GaO_6 octahedra centered at Ga(ii) atoms, sharing and linked oxygen atoms with GaO_4 tetrahedra centered at Ga(i) atoms.^{6–8} The melting point for the $\beta\text{-Ga}_2\text{O}_3$ is 2067 K, and considering this temperature of $\beta\text{-Ga}_2\text{O}_3$, the cost of production of substrates becomes cheaper than other semiconductors materials in bulk crystals, such as GaN and SiC.³

Recent works show the possibility of $\beta\text{-Ga}_2\text{O}_3$ (100) exfoliation. The [100] is the most studied and applied in this case and yielding very thin films and preserving the pristine bulk-like electronic properties, which makes it even more promising for applications in power devices.^{9,10} Kim *et al.*¹⁰ have obtained quasi-2D Ga_2O_3 flakes from bulk $\beta\text{-Ga}_2\text{O}_3$ through mechanical exfoliation, and until now, some phenomena's and properties have been studied on the $\beta\text{-Ga}_2\text{O}_3$ (100) considering the possibility of yield a 2D Ga_2O_3 , majority of this studies in a theoretical view. Su *et al.*¹¹ investigate the exfoliation process along some low index surfaces planes, and obtained exfoliation energies. It was observed the exfoliation energy for monolayer



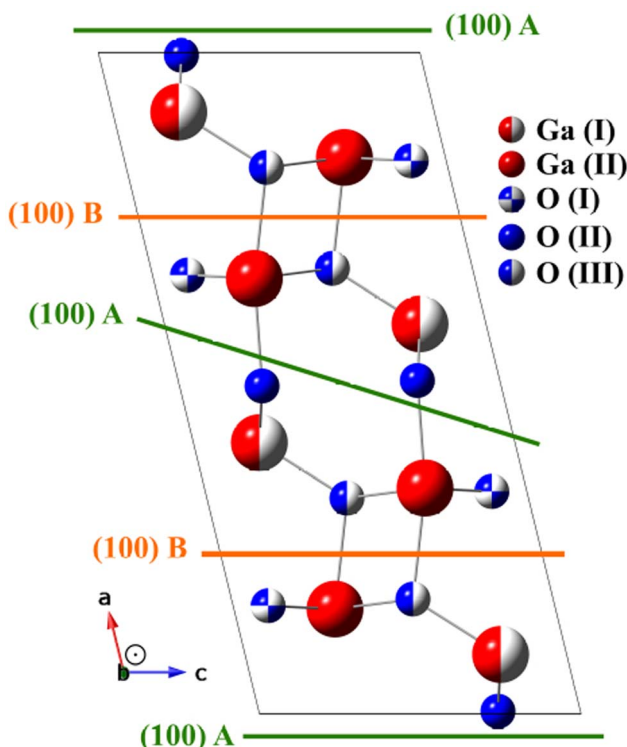


Fig. 1 Conventional unit cell of monoclinic ($C2/m$) β - Ga_2O_3 . The two different gallium (large red spheres) positions and the three inequivalent oxygen (little blue spheres) positions are illustrated. The possible stable surface termination (100) A and (100) B.

Ga_2O_3 (100) surface is lower than (010) and (001) surfaces planes, since the lattice parameters and Ga-O bonds lengths for [100] direction are larger than in the other directions, which results in the 2D monolayer being formed more readily in the (100) orientation compared to (010) and (001) orientations. Theoretical predictions about the so-called 2D Ga_2O_3 ,^{11,12} show a promising possibility of applications, since in these systems, it was observed physical properties that differ from bulk material, such as the electron mobility of bilayered β - Ga_2O_3 , being several orders of magnitude higher than β - Ga_2O_3 . This feature extends the applications of Ga_2O_3 in electronic and optoelectronic devices.^{13,14}

Bermudez⁵ performed *ab initio* theory with Hartree-Fock calculations for the slab relaxations of low index surfaces planes, such as (100), (010), (001) and (10-1). The β - Ga_2O_3 (100) was shown to have⁵ two possibilities of surface terminations (100) A and (100) B while the β - Ga_2O_3 (010) only had one surface termination. For the (010) plane it was observed the distances between Ga(i) to O(i), O(ii), and O(iii) on the surface are shorter than the bulk value. Anam *et al.*³⁸ used DFT calculations to show the 4.00 eV band gaps for Ga_2O_3 (100) with bilayer Ga_2O_3 . These results demonstrate the importance the surface terminations have on electronic properties. Pancotti *et al.*²⁰ performed XPD (X-ray photoelectron diffraction) experiments with (MSCD) multiple scattering calculation diffraction and DFT calculations. This study shows the significant displacements in the first topmost slab surface, moreover, this calculation shows an

important rumpling between gallium and oxygen atoms in the topmost surface slabs, for β - Ga_2O_3 (010).

Regarding 2D Ga_2O_3 and Bulk like β - Ga_2O_3 (100) there is some disagreement between theoretical and experimental observations,^{5,16-18} moreover the different preparation methods used for the production of the surface may promote other surfaces configurations, such as the enrichment of Ga and/or O vacancies, and consequently variations in interplanar distances at surfaces.^{5,15,19-22} For experimental studies, the ultra-high vacuum (UHV) methodologies with surface science are adequate to extract structural and electronic parameters of surface, but in the same time, it is a challenge to obtain this information straight forwardly *via in situ* experiments. Therefore, the goal of this work is to characterize the surface structure of β - Ga_2O_3 (100) *in situ* with surface science techniques.

To the best of our knowledge, there are no experimental studies with X-ray photoelectron diffraction (XPD) with the β - Ga_2O_3 (100) surface structure. In this study, we have prepared a clean β - Ga_2O_3 (100) surface which were characterized with X-ray photoelectron spectroscopy (XPS) and low-energy electron diffraction (LEED), and applied *in situ* XPD structural characterization. XPD has been strongly applied to clarify the surface structures of thin films, molecules on substrates, and two-dimensional materials systems. XPD provides information about atomic arrangements at the surface being element-sensitive and chemical state-specific. A complete understanding of the bond angles, the orientation of adsorbed molecules, and bond distances is obtained by comprehensive multiple scattering simulations.²³⁻²⁵

The results extracted from XPD experiments and simulations from the clean β - Ga_2O_3 (100) surface indicated strong relaxations in the topmost layer of surfaces, promoting almost coplanarity of the first three outmost surface layers in the model B.

Experimental section

The experiments were performed at the surface science system, equipped with Omicron HA-125HR, a hemispherical high-resolution electron analyzer with a fixed geometry, LEED optics. The sample holder was able to heat the sample up to 1300 K and the manipulator there are five degrees of freedom, 3T (x , y , z) and 2R (θ , ϕ) allowed in. The coordinates (x , y , z) moves the sample in the 3D directions and the (θ , ϕ) are the polar and azimuthal angle rotations. The β - Ga_2O_3 (100) substrate used in this study was grown by the Czochralski method and supplied by Sojitz Machinery Corporation,TM with a size of $(10 \times 10 \times 0.5)$ mm³. The analysis of the as-received sample by XPS and LEED showed small carbon peak on the surface, observed by XPS, yielding a sharp LEED pattern from the β - Ga_2O_3 (100), denoting the ordered surface. The substrate was cleaned by annealing at 800 K for 30 min in vacuum (UHV) to minimize the surface C contamination. The XPS was performed using the non-monochromatic Mg K α X-ray source. The XPS spectra were fitted using Gaussian-type functions, where each peak is composed of 50% Gaussian and 50% Lorentzian line shape with Shirley background subtracted. After the surface



characterization by LEED and XPS, the β -Ga₂O₃(100) surface was analyzed by XPD using photons from the Mg K α X-ray source. XPD measurements were performed acquiring XPS spectra from O 1s, with kinetic energy (E_k) of 723 eV core-level for the β -Ga₂O₃(100) surface. During all XPD and XPS measurements, the base pressure was kept below 7×10^{-10} mbar. XPD experiments were performed in the angle scanned mode. For the O 1s measurements, it was varied the θ polar angle in steps of 3° from 18° to 54°, while the azimuthal angle (ϕ) was varied in 3° steps from 0° to 180°, and replicated in XPD pattern (only for visualization purpose) to complete the 360°.

Theoretical XPD patterns were simulated taking into account multiple scattering in the fourth-order for the Rehr-Albers approximation^{26,27} and multiple scattering up to the sixth order. The simulations were performed once for photo-emission peak of O 1s core-level. The multiple scattering simulations considered a cluster that consisted of approximately 380 atoms with a depth range to 30 Å and a top radius of 8 Å in a paraboloid shape. The muffin-tin potential for Ga, and O atoms in their respective β -Ga₂O₃(100) bulk phases were used to obtain the phase shifts and radial matrix for the scattered electrons.

The structural parameters are determined in a fit procedure that searches for the set of parameters that optimizes the agreement between the theoretical and experimental diffraction curves, through minimization of the reliability factor R_a , defined as the difference between the experimental and the simulated diffraction patterns:

$$R_a = \sum_i \frac{(\chi_c^i(\theta, \varphi) - \chi_e^i(\theta, \varphi))^2}{\chi_c^i(\theta, \varphi)^2 + \chi_e^i(\theta, \varphi)^2}$$

The quantities χ_c^i and χ_e^i are the calculated and experimental photoelectron diffraction anisotropies, respectively. The smaller the R_a factor, the better the agreement with experiment, with $0R_a1$. A perfect agreement correspond to $R_a = 0$, no agreement is expressed by $R_a = 1$. The sum in the R_a equation is over all angles in the data base.

In the search for the lowest R_a factor, the non-structural parameters Debye temperature (T_D) and inner potential (V_0), were allowed. The interlayer distances (relaxation) were optimized for O and Ga layers (d_{12} to d_{45}), where d_{ij} is the interlayer distance between the topmost layer i and its subsequent layer j . According Fig. 1, the interlayer distances between the layers composed by Ga and O in the [100] described for a B model terminated as d_{12} distance between O(III) and O(I) layers, the d_{23} distance between O(I) and Ga(II), d_{34} distance between Ga(II) and Ga(I) and d_{45} distance between Ga(I) and O(II), for the optimized termination B, and for the termination A is described the d_{12} as distance between O(II) and Ga(I) layers, the d_{23} distance between Ga(I) and Ga(II), d_{34} distance between Ga(II) and O(I) and d_{45} distance between O(I) and O(III). The reliability factor R_a ²⁴ from the normalized XPD intensities was used to compare the experimental and simulated XPD patterns. The quantified agreement is the so-called R_a factor. The uncertainty – is about 0.05 Å considering the statistical analysis of the R_a factor.^{20,28}

Results and discussion

Fig. 2(a) shows a sharp LEED pattern at 188 eV. The LEED image shows a characteristic rectangular surface lattice and confirms the high ordering for β -Ga₂O₃(100) surface.¹⁷ Fig. 2(b) shows XPS survey spectra of β -Ga₂O₃(100) of the clean sample surface. The spectra show β -Ga₂O₃(100) characteristics peaks and do not show significant surface contamination, such as carbon located at 284.6 eV in binding energy (E_b). The surface carbon atomic concentration was estimated at 4%. The intensities for this calculation consider the relative sensitivity factors of analyzed atoms and the analyzer transmission. Fig. 3(a and b) shows the XPS for Ga 2p_{3/2} and O 1s with binding energy of peak positions at 1118 eV and 531 eV, respectively. These values are consistent with positions previously reported for β -Ga₂O₃.^{29–31}

After the characterizations of β -Ga₂O₃(100) surface by XPS and LEED, the experimental XPD patterns were collected using O 1s (Fig. 4(a)) as emitter. The theoretical XPD patterns were simulated considering the O 1s as emitter with a kinetic energy of 723 eV, where forward scattering regime dominates. For the O

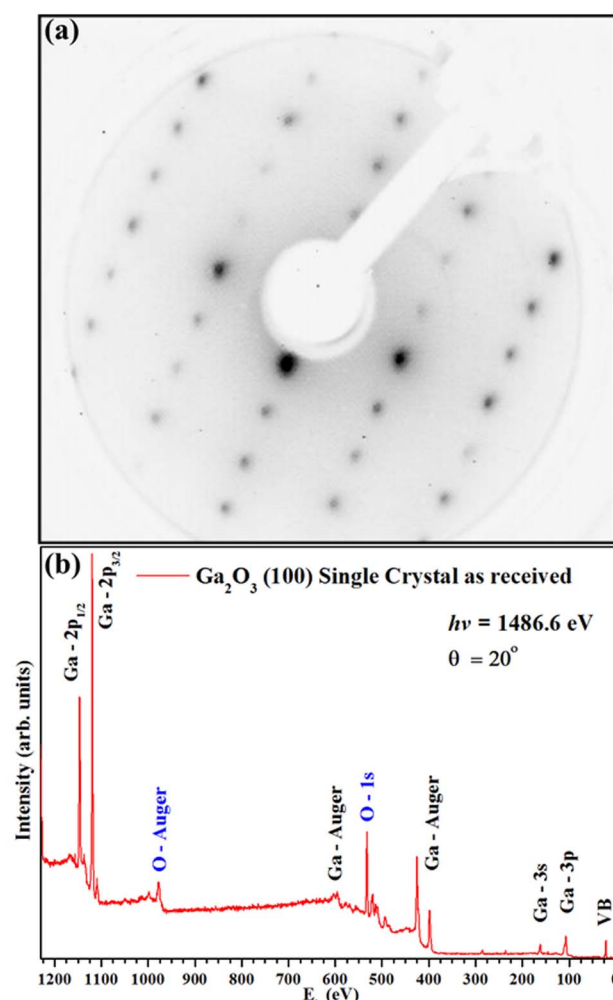


Fig. 2 (a) LEED patterns (188 eV) and (b) XPS survey spectra for the clean β -Ga₂O₃(100) sample surface.



For (a) and (b):
○ Experimental data,
— Fitting,
— Shirley Background,
 $h\nu = 1486.6 \text{ eV}$, $\theta = 20^\circ$

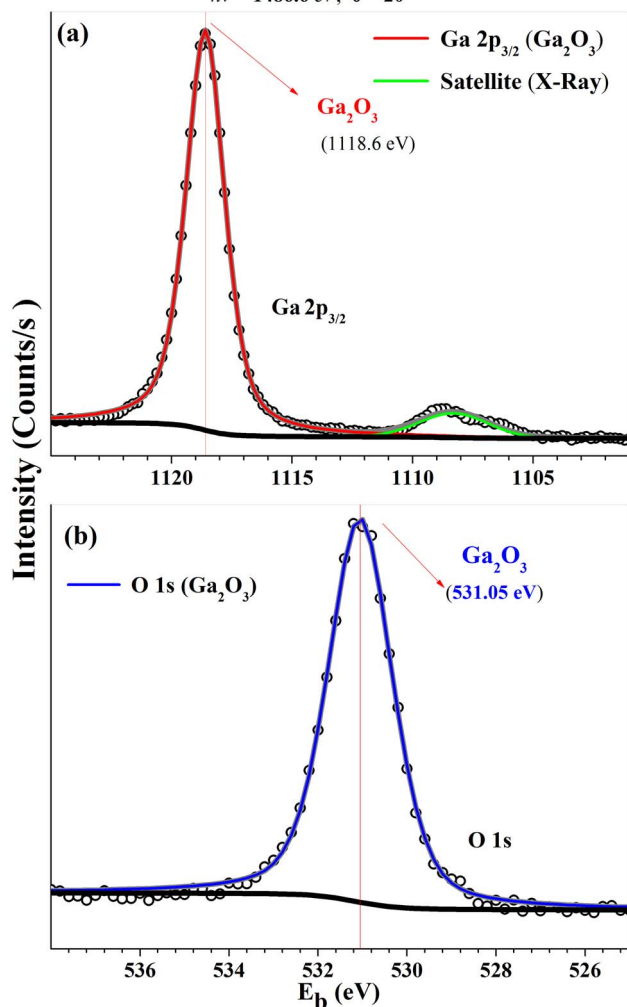


Fig. 3 HRXPS for (a) $\text{Ga} 2\text{p}_{3/2}$ and (b) O 1s XPS regions from $\beta\text{-Ga}_2\text{O}_3(100)$ sample surface.

1s XPD measurements, the forward scattering provides more sensitivity toward the position and directions of atoms on the surface structure. A higher intensity of collected photoelectrons from the surface is represented by the brighter spots in the XPD pattern. The two or four-fold symmetry is observed in all patterns, which is expected for this surface plane. These XPD patterns are in agreement with the LEED patterns shown in the Fig. 2(a).

As previously discussed there are two possibilities of termination for $\beta\text{-Ga}_2\text{O}_3(100)$,⁵ one termination called A: terminated in rows of oxygen, lying along the [010] direction with each oxygen back-bonded to two with Gallium, and B termination: where terminated in nearest-neighbor rows of gallium and oxygen atoms, each singly-unsaturated. These two terminations were proposed for the following simulations, and in the first, it were proposed the bulk value for interlayer distances, considering the vectors of the unit cell with values $a = 12.452 \text{ \AA}$,

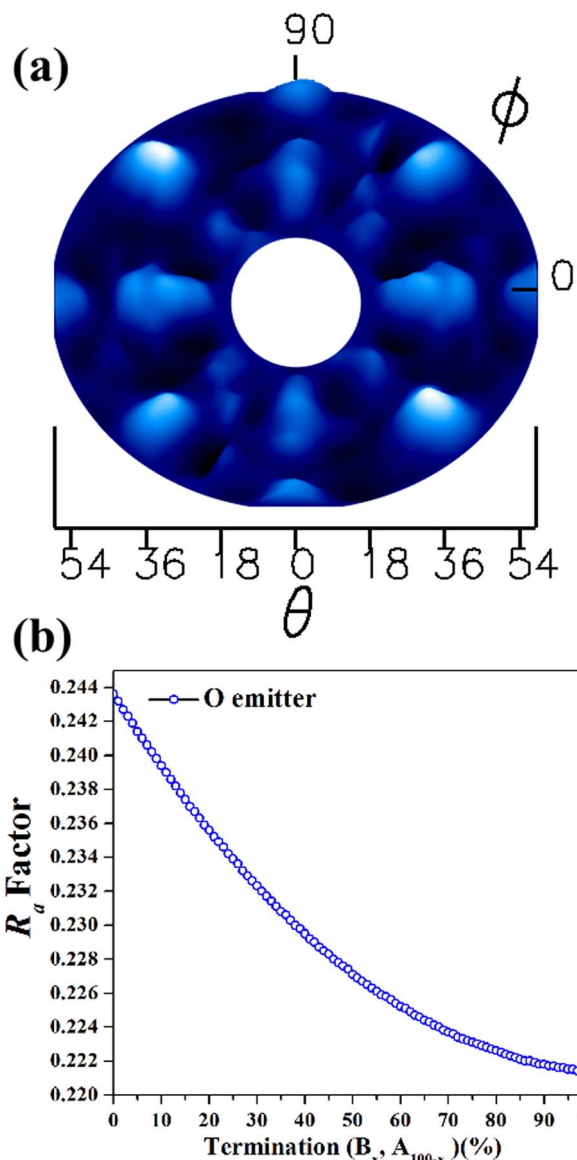


Fig. 4 (a) Experimental XPD pattern obtained from the $\beta\text{-Ga}_2\text{O}_3(100)$ sample surface for O 1s and (b) R_a factor values as a function of termination A and B in the $\beta\text{-Ga}_2\text{O}_3(100)$ surface, considering O as emitter atoms.

$b = 3.083 \text{ \AA}$; $c = 5.876 \text{ \AA}$, $\beta = 103.68^\circ$.^{32,33} The R_a factor obtained were $R_a = 0.244$ for termination called A and $R_a = 0.220$ for B termination.

Since R_a factors are close for both terminations, the following step was conducted to verify the predominance of the A and B termination on to $\beta\text{-Ga}_2\text{O}_3(100)$. Two model structures were used for the linear combination: one consisting of an A termination of $\beta\text{-Ga}_2\text{O}_3(100)$ and the other representing B termination, with bulk values for interlayer distances. The linear combination was carried out using MSCD, taking into account O 1s as emitters and considering all angles (18° to 54°). Fig. 4(b) shows the R_a factor versus linear combination for B and A termination. The smallest R_a factor in the Fig. 4(b) is referring to 100% predominance of B termination, however R_a factor

difference between A and B terminations is too small to unambiguously determine the surface predominance. The experimental work published by Lovejoy¹⁷ and co-authors showed that areas of the B termination constitute most of the surface, while areas of the A termination are small and confined to near step edges.

Considering the small difference in the R_a factor in the two surface terminations and the R_a factor value denoting good agreement between theory and experiment, we carried out the surface relaxations for both, A and B surface terminations for $\beta\text{-Ga}_2\text{O}_3(100)$.

As a first step, the non-structural parameters were relaxed, such as Inner potential (V_0) and Debye temperature (T_D). The values obtained were 750 K and 13 eV, for T_D and V_0 respectively. This is in good agreement with values previously reported in the literature.^{18,34}

After this step, relaxations of d_{12} , d_{23} , d_{34} and d_{45} interlayer distances for the $\beta\text{-Ga}_2\text{O}_3(100)$ A terminated were performed. These relaxations were performed in the same way as B termination for the search for a lower R_a factor. The intervals of interlayer distances applied during minimization process were as follows: d_{12} (0.77 Å to 1.63 Å) and d_{23} (0.04 Å to 1.07 Å), d_{34} (0.00 Å to 0.12 Å) and d_{45} (0.06 Å to 0.36 Å).

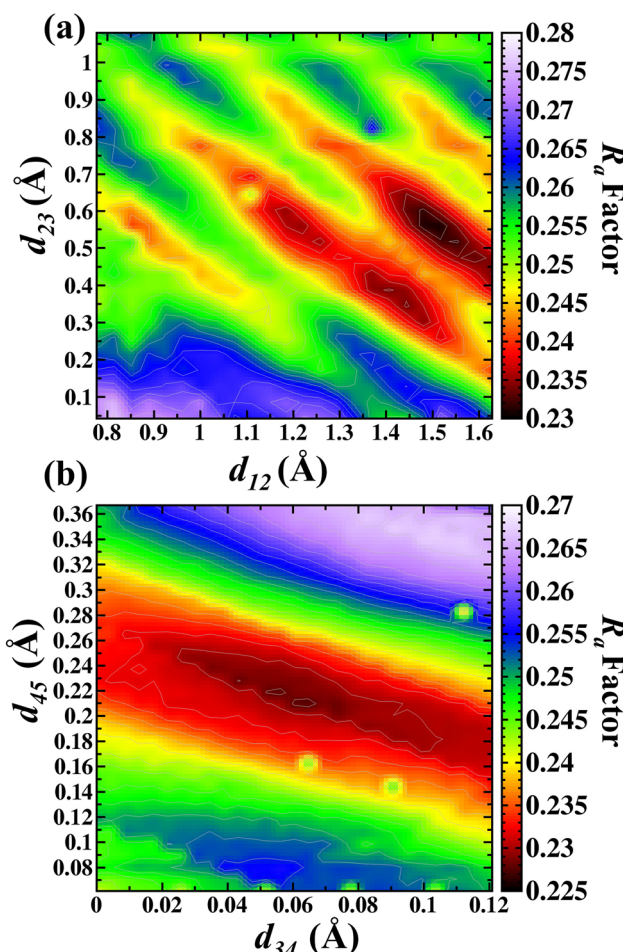


Fig. 5 Contour map in the search of lowest R_a factor for (a) d_{12} versus d_{23} and (b) d_{34} versus d_{45} for the A termination.

Fig. 5(a) shows the d_{12} and d_{23} interlayer distances in the search for the best R_a factor. The lowest R_a factor obtained was resulted in $d_{12} = 1.47$ Å (+42.6%), $d_{23} = 0.56$ Å (-32.3%). These two interlayer distances (d_{12} and d_{23}) were fixed during the d_{34} and d_{45} optimizations. The Fig. 5(b) shows the d_{34} and d_{45} interlayer distances in the search for the best R_a factor. The lowest R_a factor refer to interlayer distances $d_{34} = 0.064$ Å (+5.1%) and $d_{45} = 0.20$ Å (+71.6%). The bonding distance obtained with these structural relaxations were $\text{O}(\text{II})\text{-Ga}(\text{I})$ 2.13 Å, $\text{Ga}(\text{I})\text{-O}(\text{III})$ 1.745 Å, $\text{Ga}(\text{I})\text{-O}(\text{I})$ 1.806 Å, $\text{Ga}(\text{II})\text{-O}(\text{III})$ 1.967 Å, $\text{Ga}(\text{II})\text{-O}(\text{III})$ 1.967 Å, $\text{Ga}(\text{II})\text{-O}(\text{I})$ 2.118 Å. The R_a factor achieved for these relaxed interlayer distances was $R_a = 0.228$.

In our study the d_{12} expansion was observed, which is in contrast with previous work which showed the contraction of the outmost oxygen $\text{O}(\text{II})$ toward the $\text{Ga}(\text{I})$.⁵ It was previously shown that the d_{23} is the distance between the $\text{Ga}(\text{I})$ and $\text{O}(\text{I})$, having a contraction of 0.07 Å for this interlayer distance, toward these layers in direction to the surface.⁵ In our study the distance between $\text{Ga}(\text{I})$ and $\text{O}(\text{I})$ contract from the 0.89 Å to 0.62 Å (-29%). The distance $\text{O}(\text{I})$ and $\text{Ga}(\text{II})$ achieved in our study was from a bulk value of 0.062 Å to 0.065 Å, with an expansion of +5%. Simulations performed with the DFT calculations⁵ showed an expansion between the third and fourth atomic layer (d_{34}), represented by $\text{O}(\text{I})$ and $\text{Ga}(\text{II})$. Finally, the d_{45} or $\text{Ga}(\text{II})$ and $\text{O}(\text{III})$ layer is achieved with an expansion of 0.01 Å.⁵ In this work the distance was from 0.18 to 0.20 Å, and the observed expansion is in agreement with Bermudez.⁵

In the next step, relaxations of d_{12} , d_{23} , d_{34} and d_{45} interlayer distances for the $\beta\text{-Ga}_2\text{O}_3(100)$ surface structure, termination B model were realized. These relaxations were performed in the same way as A termination for the search of lower R_a factor. These relaxations were varied and performed at the same time in the search for the lower R_a factor, using O atoms as emitters. The relaxation optimizations were done with 0.01 Å steps for the search for d_{12} and d_{23} , and 0.05 Å steps for d_{34} and d_{45} . The limits of interlayer distances applied to the search were as follows: d_{12} and d_{23} (0.00 Å to 0.21 Å), d_{34} and d_{45} (0.15 Å to 1.54 Å).

Fig. 6(a) shows the d_{12} and d_{23} interlayer distances in the search for the best R_a factor. The lowest R_a factor obtained was for $d_{12} = 0$ Å (-100%), $d_{23} = 0.09$ Å (-50.1%). In the next step, the values obtained for d_{12} and d_{23} were then kept fixed and the optimization of the d_{34} and d_{45} interlayer distances was carried out. The Fig. 6(b) shows the d_{34} and d_{45} interlayer distances in the search for the best R_a factor. The lowest R_a factor yielded interlayer distances of $d_{34} = 1.17$ Å (+41.3%) and $d_{45} = 0.74$ Å (-28.7%). The bonding distance obtained with these structural relaxations were $\text{Ga}(\text{II})\text{-O}(\text{III})$ 1.968 Å, $\text{Ga}(\text{II})\text{-O}(\text{I})$ 2.102 Å, $\text{Ga}(\text{I})\text{-O}(\text{I})$ 2.04 Å, $\text{Ga}(\text{I})\text{-O}(\text{II})$ 1.711 Å and $\text{Ga}(\text{I})\text{-O}(\text{III})$ 2.06 Å. The R_a factor achieved for these relaxed interlayer distances was R_a factor: 0.204.

The surface plane (100) with B termination, for $\beta\text{-Ga}_2\text{O}_3$ is the most stable surface termination compared with the other terminations for the low index planes, such as (100) A, (010) and (001). Other experimental^{18,35} and theoretical^{13,21} works find this same behavior. Our results agree with these studies since the lowest R_a factor ($R_a = 0.220$) for bulk interlayer distances shows



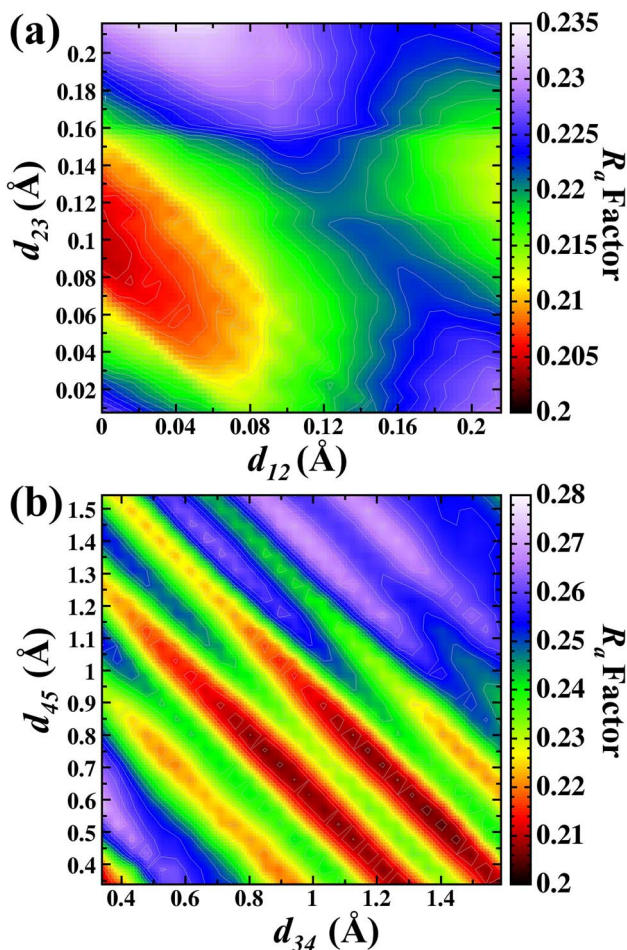


Fig. 6 Contour map in the search of lowest R_a factor for (a) d_{12} versus d_{23} and (b) d_{34} versus d_{45} for the B termination.

that the most likely termination describing the surface is $\beta\text{-Ga}_2\text{O}_3(100)$ B.

The interlayer differences in this study differ from those found previously.⁵ Considering the behavior of displacements for O(I), O(III) and Ga(II) for the study of Bermudez, our results show similar coplanarity in the topmost surface. Bermudez has shown an expansion for the d_{34} , and a little contraction between the distances formed by Ga(II) and Ga(I), represented by d_{34} .

The bonding distances obtained in our study show slightly larger values compared with previous work.^{5,35} Additionally,

Table 1 Interlayer distances d_{ij} up to the five atomic layer from the surface as determined by the O 1s XPD simulations. All values are given in Å. Negative or positive percentage values indicate a contraction or expansion displacement relative to the bulk

Interlayer distance	A – terminated		B – terminated	
	$R_a = 0.228$		$R_a = 0.204$	
d_{12}	1.47(+42.6)		0(-100)	
d_{23}	0.56(-32.3)		0.09(-50.1)	
d_{34}	0.064(+5.1)		1.17(+41.3)	
d_{45}	0.20(+71.6)		0.74(-28.7)	

similar expansions in the bonding distance was observed by Barman *et al.*,⁹ who used *ab initio* calculations to study $\beta\text{-Ga}_2\text{O}_3(100)$.⁹

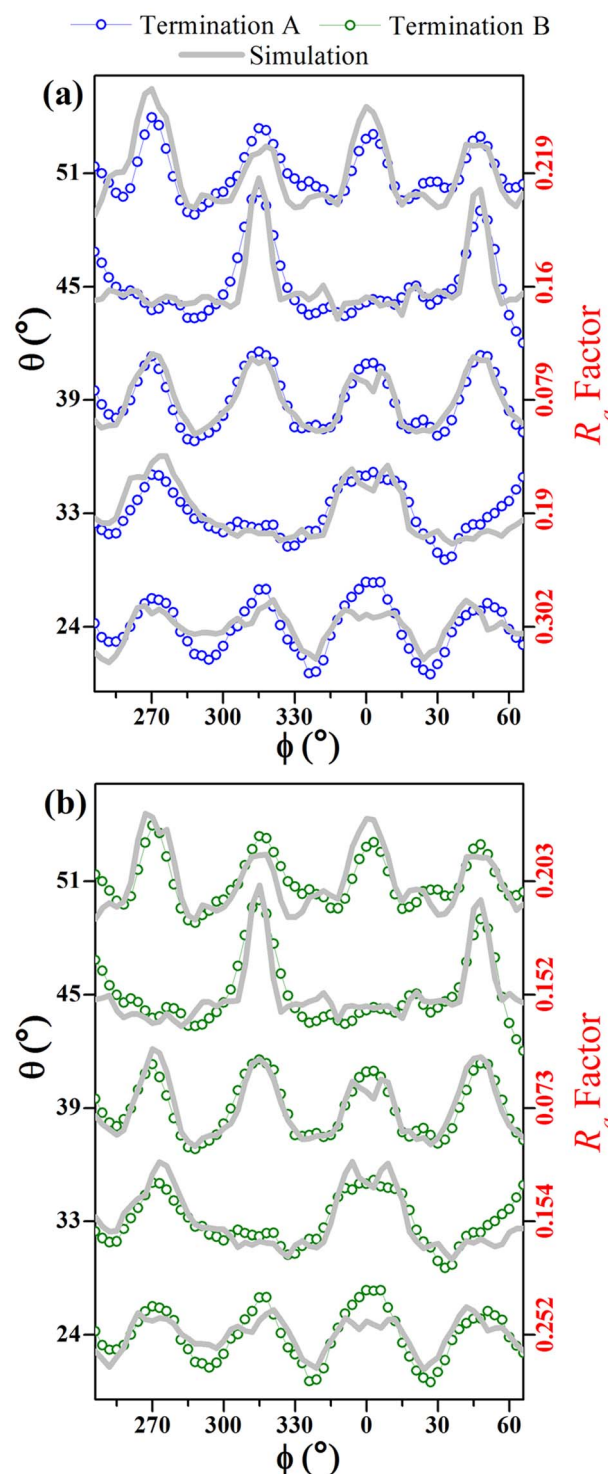


Fig. 7 Simulated (gray lines) and experimental (open points) azimuthal scans for selected polar angles (for $\theta = 24^\circ, 33^\circ, 39^\circ, 45^\circ$, and 51°) for (a) termination A (blue open points), and (b) termination B (green open points) model structure surface for O as emitter atom from $\beta\text{-Ga}_2\text{O}_3(100)$ surface.

Changes in the atomic interlayer distances of the Ga_2O_3 for the first five atomic layers as determined by the O 1s XPD simulations are shown in the Table 1. Negative values indicate a contraction in the interlayer distance, whereas positive values indicate an expansion into the relative bulk value. All displacements are in Å.

Fig. 7 compares simulated and experimental azimuthal scans, from 246° to 66° , at selected polar angles, for both A and B model terminations. It demonstrates excellent agreement for the curves measured at polar angles between 24° and 51° . Model B shows lower R_a factors for all range of angles (bulk and surface sensitive).

Of the terminations studied in these simulations have global R_a -factors below 0.23, which is not sufficiently different for distinguishing between the terminations, even though they are clearly consistent with the $\beta\text{-Ga}_2\text{O}_3(100)$ structure. Since the experiment in Fig. 4(a) involves polar angles from 18° to 54° , the small polar angle data ($\leq 39^\circ$), which reflect internal layers, mask those for the more grazing angles, which are surface sensitive. In order to demonstrate this, we show, in Fig. 7(a and b), the R_a -factor for the higher (*i.e.*, more grazing) polar angles ($\geq 39^\circ$) calculated by summing over the azimuthal intensities for each polar angle. The different curves are labeled according to our termination nomenclature, as in Fig. 1. From Fig. 7, it is very clear that this more surface sensitive data allows us to distinguish between the different termination models. With this additional information it appears that the surface is most likely B terminated.

The simulated XPD patterns for all polar angles (18° to 54°) are shown in Fig. 8(a) for the proposed $\beta\text{-Ga}_2\text{O}_3(100)$ -A surface termination and Fig. 8(b) for $\beta\text{-Ga}_2\text{O}_3(100)$ -B surface termination, where O 1s was used as emitter atom. For these models, we considered all relaxations which yielded R_a factors of 0.228 and 0.204 for A and B terminated surfaces respectively. The study of monoclinic surface structure by XPD simulations is quite a challenging task, since the description of periodicity of layers in the $\beta\text{-Ga}_2\text{O}_3$ [100] is low, moreover normally the oxide metal and semiconductor materials have defects and vacancies for both anions or cations on the surface.^{22,23,36,37} Despite the difficulty results in this work showed good agreement between theoretical proposed models and experiment.

Fig. 9(a) displays the $\beta\text{-Ga}_2\text{O}_3$ (100)-A surface for the final structural model for termination A. For model A, d_{12} and d_{34} and d_{45} interlayer distances are followed by an expansion and d_{23} contraction. For model B displayed in the Fig. 9(b), d_{12} and d_{45} interlayer distances is observed contraction and expansion for d_{23} and d_{34} , emerging almost coplanarity for the first three layers due to the displacements in the d_{12} , d_{23} and d_{34} .

Regarding STM study,^{4,11,38} the observed surface morphology was associated with large and small terraces, with 1.5 Å bigger height for the (100) B termination and another small terrace for the (100) A termination. These experiments are not element specific and cannot differentiate the A or B termination at the surface clearly. This work showed which types of atoms that form each type of termination of the surface of the $\beta\text{-Ga}_2\text{O}_3$ [100]. The (100)A surface is terminated with O(*ii*) atoms and (100)B is terminated with both Ga(*ii*), O(*i*), and O(*iii*) atoms.

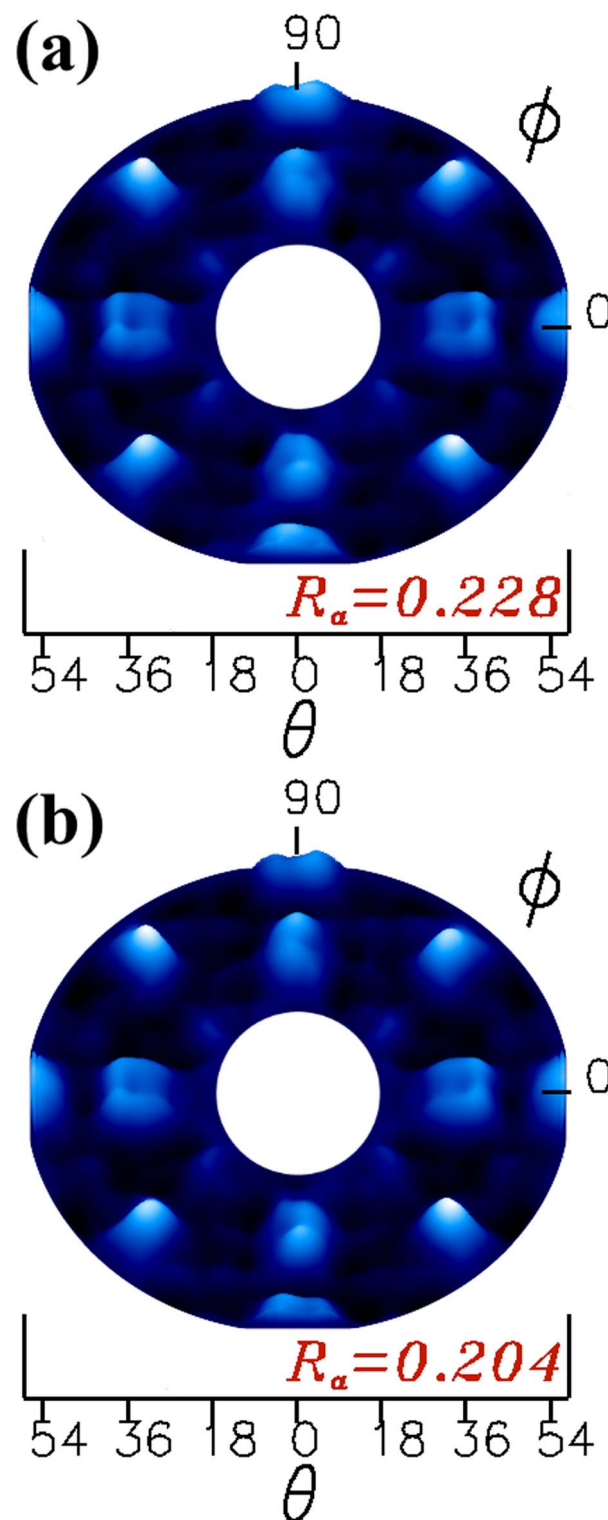


Fig. 8 Theoretical XPD patterns obtained from the $\beta\text{-Ga}_2\text{O}_3(100)$ surface models, for termination (a) A and (b) B.

Theoretical studies show the most energetically favorable termination at the $\beta\text{-Ga}_2\text{O}_3$ (100) surface is the termination (100)B, mainly because the Ga–O are strong covalent bonds at (100)B termination.^{3,10}



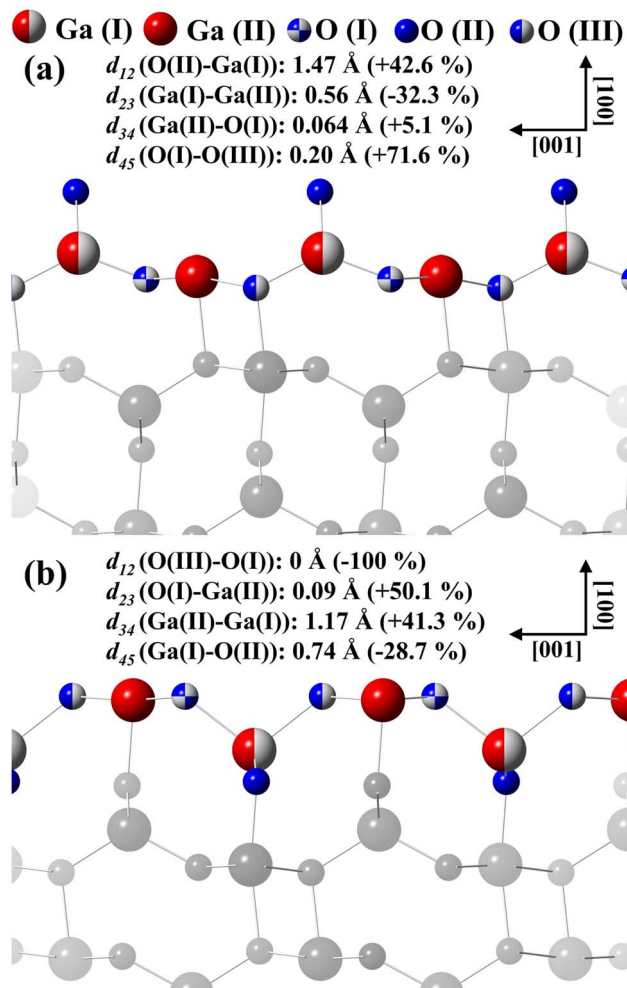


Fig. 9 Interlayer distances calculated for the models with termination (a) A and (b) B proposed to describe the $\beta\text{-Ga}_2\text{O}_3(100)$ surfaces.

Therefore, the knowledge of the structural parameters for the $\beta\text{-Ga}_2\text{O}_3(100)$ surface at the atomic level is key for understanding electronic properties previously observed in the theoretical studies on to $\beta\text{-Ga}_2\text{O}_3(100)$ surface. Further investigations considering the results obtained here may enlighten other special phenomena such as ferromagnetism.

Conclusions

A systematic and precise *in situ* XPD study of the $\beta\text{-Ga}_2\text{O}_3(100)$ surface was presented here. The LEED and XPS characterization indicated well-ordered surface structures. XPD and structural information was provided by simulations for the model's systems A and B type terminations. The linear combination for B and A termination indicate that the surface termination is 100% predominance of B termination. Model A and B present significant displacements in the interlayer distances of the outermost $\text{Ga}_2\text{O}_3(100)$ in comparison to the bulk value.

Moreover, MSCD simulations indicated the formation of almost coplanarity of layers in the proposed model B. The low R_a factor provides the reliability of the results for the two models

but the little difference in the R_a factor does not allow the choice of a specific model (A or B) to describe the predominance in the surface. The determination of the distances between atomic planes of the two models proposed here in this work allows knowing and controlling the surface structure, and this raises the opportunity to modify the physical properties of these nanomaterials, in comparison with the bulk structure. The optimized XPD simulations of the surface structure lead to average R_a -factor of 0.204, implying a good agreement between experimental results and simulations. Properties such as thermal and electrical conductivity are strongly influenced by the geometric parameters of these materials and these properties are essential for the manufacture of electronic devices.

Author contributions

Alex Sandre Kilian: writing – original draft, methodology, formal analysis, software, investigation and visualization. Abner de Siervo: methodology, writing – review & editing, resources and software. Guilherme Jean P. Abreu: investigation, writing – review & editing, methodology. Mayron Silva Castro: investigation, editing, and methodology. Tyson Back: methodology, writing – review & editing, resources and software. Alexandre Pancotti: project administration, writing–review & editing, and funding acquisition.

Conflicts of interest

There are no conflicts to declare.

Acknowledgements

A. S. K. thanks USA Air Force for the resource and his PostDoc fellowship. We would like to acknowledge Dr Ali Sayir for useful discussions. This material is based upon work supported by the Air Force Office of Scientific Research (AFOSR) under award FA9550-21-1-0440 and Conselho Nacional de Desenvolvimento Científico e Tecnológico – CNPq programme 310774/2020-9 under grant agreement.

Notes and references

- 1 S. Roy, A. Bhattacharyya, P. Ranga, H. Splawn, J. Leach and S. Krishnamoorthy, *IEEE Electron Device Lett.*, 2021, **42**, 1140–1143.
- 2 J. Zhang, J. Shi, D.-C. Qi, L. Chen and K. H. L. Zhang, *APL Mater.*, 2020, **8**, 020906.
- 3 D. Guo, Q. Guo, Z. Chen, Z. Wu, P. Li and W. Tang, *Mater. Today Phys.*, 2019, **11**, 100157.
- 4 H. Xue, Q. He, G. Jian, S. Long, T. Pang and M. Liu, *Nanoscale Res. Lett.*, 2018, **13**, 290.
- 5 V. M. Bermudez, *Chem. Phys.*, 2006, **323**, 193–203.
- 6 B. R. Tak, S. Kumar, A. K. Kapoor, D. Wang, X. Li, H. Sun and R. Singh, *J. Phys. D: Appl. Phys.*, 2021, **54**, 453002.
- 7 S. Ghose, S. Rahman, L. Hong, J. S. Rojas-Ramirez, H. Jin, K. Park, R. Klie and R. Droopad, *J. Appl. Phys.*, 2017, **122**, 095302.



8 E. Ahmadi and Y. Oshima, *J. Appl. Phys.*, 2019, **126**, 160901.

9 S. K. Barman and M. N. Huda, *Phys. Status Solidi RRL*, 2019, **13**, 1800554.

10 J. Kim, S. Oh, M. A. Mastro and J. Kim, *Phys. Chem. Chem. Phys.*, 2016, **18**, 15760–15764.

11 J. Zhao, X. Wang, H. Chen, Z. Zhang and M. Hua, *Chem. Mater.*, 2022, **34**, 3648–3658.

12 J. Zhao, X. Huang, Y. Yin, Y. Liao, H. Mo, Q. Qian, Y. Guo, X. Chen, Z. Zhang and M. Hua, *J. Phys. Chem. Lett.*, 2021, **12**, 5813–5820.

13 J. Su, R. Guo, Z. Lin, S. Zhang, J. Zhang, J. Chang and Y. Hao, *J. Phys. Chem. C*, 2018, **122**, 24592–24599.

14 W. Ding, J. Zhu, Z. Wang, Y. Gao, D. Xiao, Y. Gu, Z. Zhang and W. Zhu, *Nat. Commun.*, 2017, **8**, 14956.

15 M. Busch, E. Meyer, K. Irmscher, Z. Galazka, K. Gärtner and H. Winter, *Appl. Phys. Lett.*, 2014, **105**, 051603.

16 M. Mohamed, I. Unger, C. Janowitz, R. Manzke, Z. Galazka, R. Uecker and R. Fornari, *J. Phys.: Conf. Ser.*, 2011, **286**, 012027.

17 T. C. Lovejoy, E. N. Yitamben, N. Shamir, J. Morales, E. G. Villora, K. Shimamura, S. Zheng, F. S. Ohuchi and M. A. Olmstead, *Appl. Phys. Lett.*, 2009, **94**, 081906.

18 P. Mazzolini, A. Falkenstein, C. Wouters, R. Schewski, T. Markurt, Z. Galazka, M. Martin, M. Albrecht and O. Bierwagen, *APL Mater.*, 2020, **8**, 011107.

19 S. Jang, S. Jung, K. Beers, J. Yang, F. Ren, A. Kuramata, S. J. Pearton and K. H. Baik, *J. Alloys Compd.*, 2018, **731**, 118–125.

20 A. Pancotti, T. C. Back, W. Hamouda, M. Lachheb, C. Lubin, P. Soukiassian, J. Boeckl, D. Dorsey, S. Mou, T. Asel, G. Geneste and N. Barrett, *Phys. Rev. B*, 2020, **102**, 245306.

21 T. Liu, Z. Feng, Q. Li, J. Yang, C. Li and M. Dupuis, *Chem. Mater.*, 2018, **30**, 7714–7726.

22 A. S. Kilian, G. J. Abreu, A. de Siervo, R. Landers and J. Morais, *CrystEngComm*, 2022, **24**, 2270–2279.

23 A. S. Kilian, F. Bernardi, A. Pancotti, R. Landers, A. de Siervo and J. Morais, *J. Phys. Chem. C*, 2014, **118**, 20452–20460.

24 A. S. Kilian, A. Pancotti, R. Landers, A. de Siervo and J. Morais, *CrystEngComm*, 2014, **16**, 9291–9298.

25 Y. Chen, F. J. García de Abajo, A. Chassé, R. X. Ynzunza, A. P. Kaduwela, M. A. Van Hove and C. S. Fadley, *Phys. Rev. B: Condens. Matter Mater. Phys.*, 1998, **58**, 13121.

26 J. J. Rehr and R. C. Albers, *Phys. Rev. B: Condens. Matter Mater. Phys.*, 1990, **41**, 8139–8149.

27 J. B. Pendry, *J. Phys. C: Solid State Phys.*, 1980, **13**, 937–944.

28 P. Chen, K. Li, B. Lei, L. Chen, W. Cui, Y. Sun, W. Zhang, Y. Zhou and F. Dong, *ACS Appl. Mater. Interfaces*, 2021, **13**, 50975–50987.

29 D. A. Zatsepин, D. W. Boukhvalov, A. F. Zatsepин, Y. A. Kuznetsova, D. Gogova, V. Y. Shur and A. A. Esin, *Superlattices Microstruct.*, 2018, **120**, 90–100.

30 M. Mulazzi, F. Reichmann, A. Becker, W. M. Klesse, P. Alippi, V. Fiorentini, A. Parisini, M. Bosi and R. Fornari, *APL Mater.*, 2019, **7**, 022522.

31 Q. Chen, Y. Zhang, T. Zheng, Z. Liu, L. Wu, Z. Wang and J. Li, *Nanoscale Adv.*, 2020, **2**, 2705–2712.

32 A. Usseinov, Z. Koishbayeva, A. Platonenko, V. Pankratov, Y. Suchikova, A. Akilbekov, M. Zedorovets, J. Purans and A. I. Popov, *Materials*, 2021, **14**, 7384.

33 J. Su, J. Zhang, R. Guo, Z. Lin, M. Liu, J. Zhang, J. Chang and Y. Hao, *Mater. Des.*, 2019, **184**, 108197.

34 K. Iwaya, R. Shimizu, H. Aida, T. Hashizume and T. Hitosugi, *Appl. Phys. Lett.*, 2011, **98**, 142116.

35 E. A. Gonzalez, P. V. Jasen, A. Juan, S. E. Collins, M. A. Baltanás and A. L. Bonivardi, *Surf. Sci.*, 2005, 575, 171–180.

36 G. J. P. Abreu, A. Pancotti, L. H. Lima, R. Landers and A. Siervo, *J. Nanopart. Res.*, 2013, **15**, 1–10.

37 A. Pancotti, A. de Siervo, M. Carazzolle, R. Landers and G. Kleiman, *Top. Catal.*, 2011, **54**, 90–96.

38 B. Anam and N. Gaston, *ChemPhysChem*, 2021, **22**, 2362–2370.

